RCS OF TERMINATED PARALLEL-PLATE WAVEGUIDE CAVITIES WITH MATERIAL LOADING

Shoichi Koshikawa and Kazuya Kobayashi
Department of Electrical and Electronic Engineering, Chuo University
1-13-27 Kasuga, Bunkyo-ku, Tokyo 112, Japan

Analysis of the diffraction by open-ended metallic waveguide cavities has been of great interest recently in connection with the prediction and reduction of the radar cross section (RCS) of a target [1]. Some of the cavity diffraction problems have been analyzed thus far using the two typical methods, namely the waveguide modal approach [2] and the high-frequency ray techniques [2, 3]. However, it appears that complete solutions to the diffraction by open cavities using function-theoretic methods based on rigorous wave theory, which are uniformly valid for arbitrary dimensions of the cavity, have not yet been established. In [4], as an example of simple two-dimensional cavity structures, we have considered a parallel-plate waveguide cavity with a planar termination at the open end and solved rigorously the diffraction of a plane electromagnetic wave by means of the Wiener–Hopf technique. In this paper, as a generalization to the problem treated in the previous paper, we shall analyze the plane wave diffraction by a terminated parallel-plate waveguide cavity with material loading using the Wiener–Hopf technique. Analytical details of the problem have already been reported elsewhere [5, 6] and hence, we shall here mainly focus on presenting numerical results of the RCS to discuss the scattering characteristics of the cavity in detail.

The geometry of the cavity is shown in Fig. 1, where ϕ^i is the incident field of either E polarization or H polarization. The medium inside the cavity is characterized by the relative permittivity ε_r and the relative permeability μ_r. The cavity plates are assumed to be infinitely thin, perfectly conducting, and uniform in the y-direction. In view of the geometry and the characteristics of the incident field, this is a two-dimensional problem. Introducing the Fourier transform for the unknown scattered field and applying the boundary conditions appropriately in the transform domain, this problem is formulated in terms of two simultaneous Wiener–Hopf equations satisfied by six unknown functions. These Wiener–Hopf equations are solved exactly via an application of the factorization and decomposition procedure. However, the solution is formal since branch-cut integrals with unknown integrands and an infinite number of unknowns are involved. Employing a rigorous asymptotics with the aid of the edge condition, an explicit form of the approximate solution is derived. The scattered field

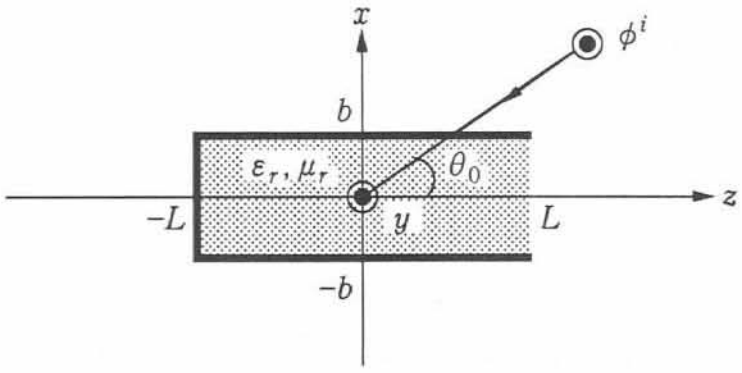

Fig. 1. Geometry of the problem.

inside and outside the cavity is further evaluated by taking the Fourier inverse of the solution in the transform domain. The field inside the cavity is expressed as the transmitted *TE* and *TM* modes for the *E* and *H* polarizations, respectively, whereas for the region outside the cavity, the scattered far field is deduced using the saddle point method.

Figures 2 and 3 are numerical examples of the monostatic RCS versus the incident angle θ_0 for the *E* polarization, where the results are plotted only for the range $0° \leqq \theta_0 \leqq 180°$ since the cavity structure is symmetric along the z-axis. Two different values of the ratio L/b are chosen as 1.0 and 2.0 in Fig. 2 and Fig. 3, respectively. In order to investigate the scattering mechanism for each value of L/b over a wide frequency range, numerical computations have been carried out for three typical values of the cavity aperture, namely, $2b = \lambda$, 5λ, and 10λ. The material parameter in each example is $\varepsilon_r = 2.5 + i1.25$, $\mu_r = 1.6 + i0.8$, and the results for no material loading have also been added by dashed lines to clarify the effect of lossy material loading inside the cavity. The results for the *H* polarization with the choice of the same parameters are shown in Figs. 4 and 5.

From the figures, we observe that there are three particular peaks at $\theta_0 = 0°$, 90°, and 180° corresponding to the specularly reflected fields from the cavity surface, which can be easily predicted by the geometrical optics. On comparing the curves with and without material loading, we notice that the RCS characteristics for the range $90° \leqq \theta_0 \leqq 180°$ are almost the same, but remarkable differences can be seen for $0° \leqq \theta_0 \leqq 90°$. For no material loading, the monostatic RCS is smoothly varying and exhibits fairly large values within the range $0° \leqq \theta_0 \leqq 70°$ due to the reradiation of the waveguide modal fields, but the reradiation within this range is reduced for the case of material loading. This is because for $0° \leqq \theta_0 \leqq 90°$, the aperture of the cavity is in the illuminated region against the incident field and hence, the scattered field is then strongly affected by the lossy material loading inside the cavity. We also find by comparing the three curves of $2b = \lambda$, 5λ, and 10λ that the reduction is noticeable for larger cavities. This shows that a good RCS reduction can be achieved over a wide range of the incident angle for large cavities by lossy material loading. Comparing the results for the *E* and *H* polarizations, it is seen that the characteristics for two different polarizations show similar features for $2b = 10\lambda$, whereas differences can be observed for smaller cavities. The method of solution established in [5, 6] and this paper is based on rigorous wave theory via the Wiener–Hopf technique and hence, all the results presented here are highly accurate.

Acknowledgements

The authors would like to thank Professor Kazuo Horiuchi of Waseda University for many helpful discussions. They are also indebted to Miss Akiko Sawai, a graduate school student at Chuo University, for assisting in the preparation of the manuscript.

References

[1] W. R. Stone, Ed., *Radar Cross Sections of Complex Objects*, IEEE Press, New York, 1990.

[2] H. Ling, S.-W. Lee, and R.-C. Chou, "High-frequency RCS of open cavities with rectangular and circular cross sections," *IEEE Trans. Antennas Propagat.*, Vol. AP-37, 648–654, 1989.

[3] P. H. Pathak and R. J. Burkholder, "Modal, ray, and beam techniques for analyzing the EM scattering by open-ended waveguide cavities," *IEEE Trans. Antennas Propagat.*, Vol. AP-37, 635–647, 1989.

[4] K. Kobayashi and A. Sawai, "Plane wave diffraction by an open-ended parallel plate waveguide cavity," *J. Electromagnetic Waves Applics.*, Vol. 6, 1992 (to be published).

[5] K. Kobayashi, "Diffraction by an open-ended parallel plate waveguide cavity with dielectric/ferrite loading: I. The case of *E* polarization," *IEEE AP-S Symposium Digest*, 1054–1057, 1991.

[6] S. Koshikawa and K. Kobayashi, "Diffraction by an open-ended parallel plate waveguide cavity with dielectric/ferrite loading: II. The case of *H* polarization," *IEEE AP-S Symposium Digest*, 1058–1061, 1991.

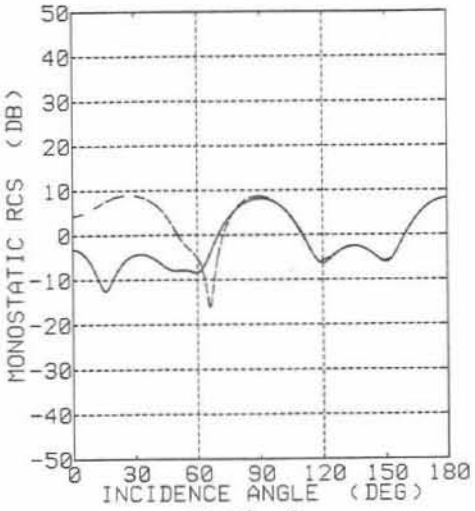

(a) $2b = \lambda$.

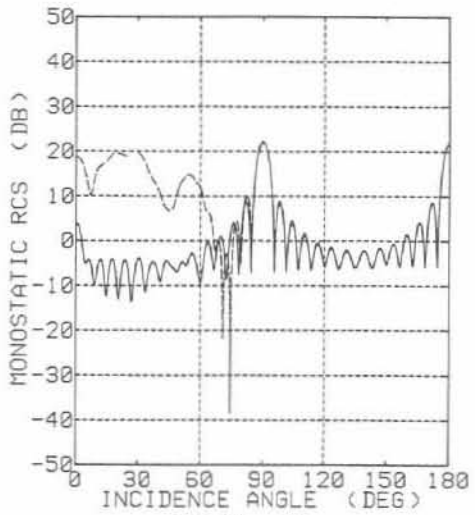

(b) $2b = 5\lambda$.

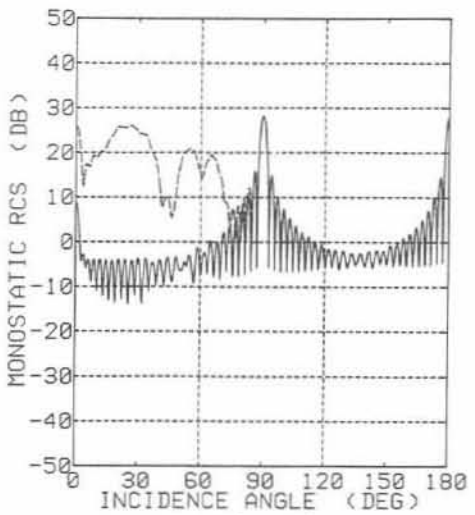

(c) $2b = 10\lambda$.

Fig. 2. Monostatic RCS σ/λ [dB] for $L/b = 1.0$ (E polarization).
Solid lines and dashed lines denote the cases for material loading with $\varepsilon_r = 2.5+i1.25$, $\mu_r = 1.6+i0.8$ and no material loading, respectively.

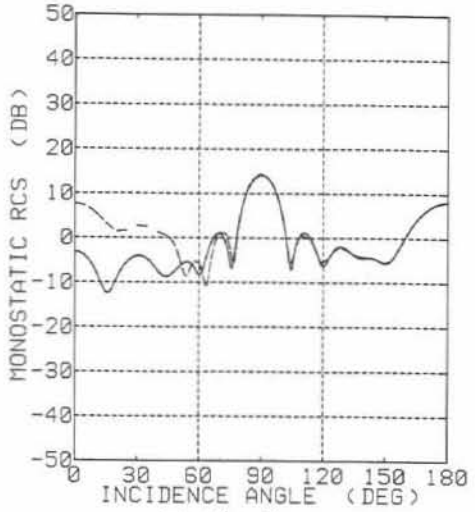

(a) $2b = \lambda$.

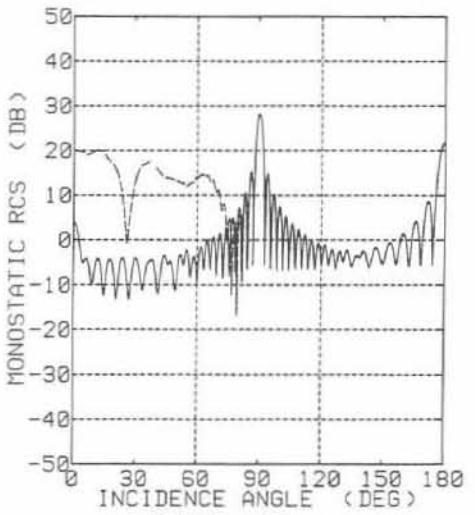

(b) $2b = 5\lambda$.

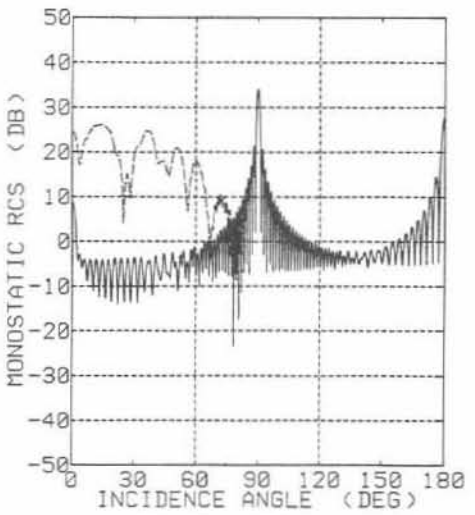

(c) $2b = 10\lambda$.

Fig. 3. Monostatic RCS σ/λ [dB] for $L/b = 2.0$ (E polarization).
Solid lines and dashed lines denote the cases for material loading with $\varepsilon_r = 2.5+i1.25$, $\mu_r = 1.6+i0.8$ and no material loading, respectively.

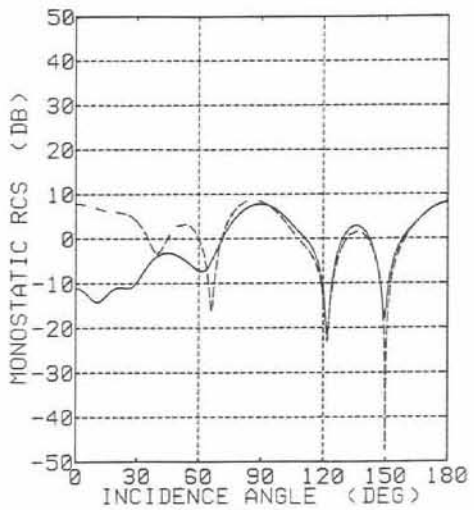

(a) $2b = \lambda$.

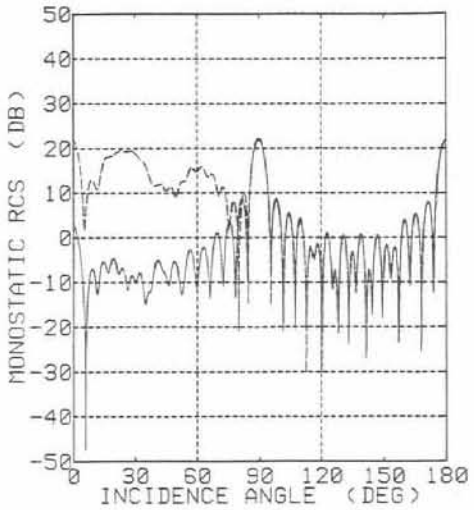

(b) $2b = 5\lambda$.

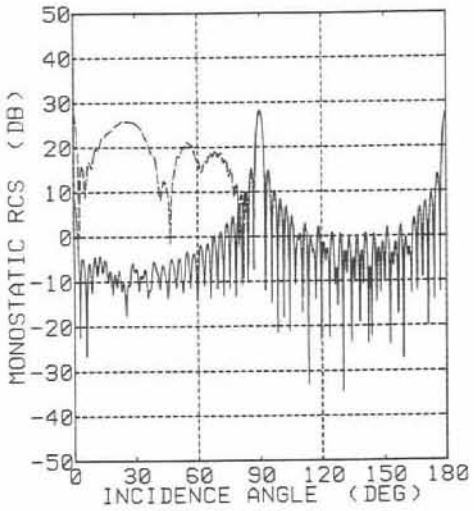

(c) $2b = 10\lambda$.

Fig. 4. Monostatic RCS σ/λ [dB] for $L/b = 1.0$ (H polarization). Solid lines and dashed lines denote the cases for material loading with $\varepsilon_r = 2.5+i1.25$, $\mu_r = 1.6+i0.8$ and no material loading, respectively.

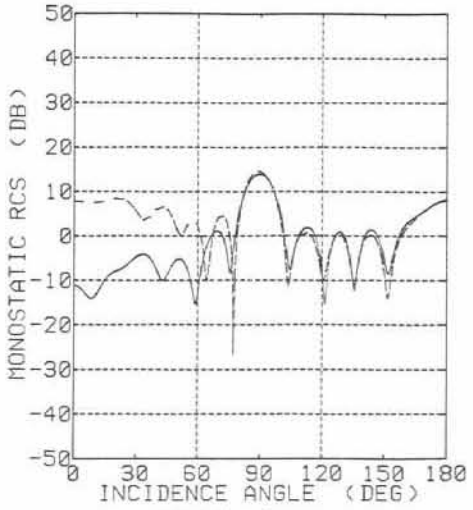

(a) $2b = \lambda$.

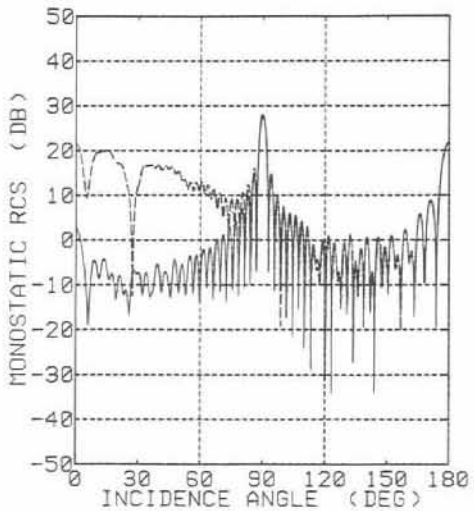

(b) $2b = 5\lambda$.

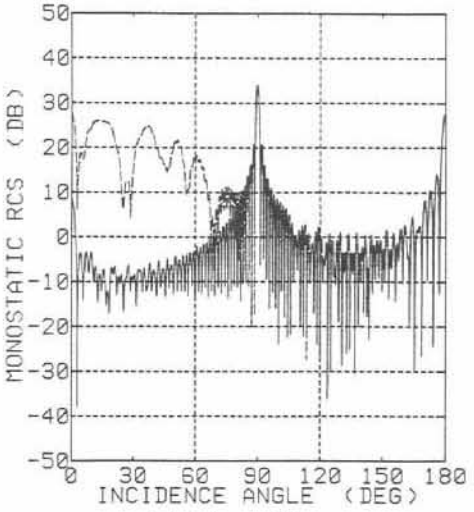

(c) $2b = 10\lambda$.

Fig. 5. Monostatic RCS σ/λ [dB] for $L/b = 2.0$ (H polarization). Solid lines and dashed lines denote the cases for material loading with $\varepsilon_r = 2.5+i1.25$, $\mu_r = 1.6+i0.8$ and no material loading, respectively.